articles

molecular pharmaceutics

A Novel Type of Dual-Modality Molecular Probe for MR and Nuclear Imaging of Tumor: Preparation, Characterization and in Vivo Application

Shujie Liu,[†,‡] Bing Jia,[‡,§] Ruirui Qiao,[†,‡] Zhi Yang,[||] Zilin Yu,[§] Zhaofei Liu,[§] Kan Liu,[⊥] Jiyun Shi,[§] Han Ouyang,[⊥] Fan Wang,[*,§] and Mingyuan Gao[*,†]

Institute of Chemistry, CAS, Bei Yi Jie 2, Beijing 100190, China, Medical Isotopes Research Center, Peking University, Xueyuan Road 38, Beijing 100191, China, Cancer Hospital of Chinese Academy of Medical Sciences, Pan Jia Yuan Nan Li 17, Beijing 100021, China, and Oncology School of Peking University, Fu Cheng Lu 52, 100036, China

Received October 30, 2008; Accepted June 15, 2009

Abstract: A novel dual-modality molecular probe composed of biocompatible Fe_3O_4 nanocrystal, monoclonal antibody and radionuclide was designed and prepared. All functional components in the dual-modality molecular probe, i.e., Fe_3O_4, PEG, mAb 3H11 and ^{125}I, were chemically bonded together for forming a stable molecular probe. Systematic *in vitro* experiments were carried out for evaluating the biological activity of the antibody in the targeting probe. A series of *in vivo* experiments were performed based on the dual-modality imaging probe for detecting xenografted tumors in nude mice by MRI and γ-imaging techniques. The pharmacokinetics of the dual-modality molecular probe in tumor-bearing nude mice was studied.

Keywords: Dual-modality molecular probe; MRI; nuclear imaging; Fe_3O_4 nanocrystals; tumor

Introduction

Molecular imaging has become a booming area as it will surely offer revolutionary tools not only for fundamental diagnostic studies but also for clinical applications.[1−3] Over the past decade, different types of molecular imaging probes have been developed for fluorescence imaging,[4,5] magnetic resonance imaging (MRI),[2,6−10] nuclear imaging,[11,12] etc. Among them, nanoparticle-based molecular probes have become more and more attractive. First, the size-dependent physical properties of nanoparticles such as fluorescent quantum dots and magnetic iron oxide nanoparticles are potentially useful for acquiring detailed physiological information at the cellular level *in vitro* and even *in vivo*.[5,13] Second, in comparison with small molecular imaging agents, nanoparticles injected into the bloodstream present very special size- and surface-dependent *in vivo* behaviors governed by the uptake effects of reticuloendothelial system (RES), thus offering new possibilities for disease diagnosis via different passive targeting modes.[14,15] Third, the nanoparticles can provide multiple surface binding sites for further attaching various types of bioactive molecules, consequently

* To whom correspondence should be addressed. M.G.: Mailing address, Institute of Chemistry, CAS, Bei Yi Jie 2, Zhong Guan Cun, Beijing 100190, China. Fax: 86-10-82613214. Tel: 86-10-82613214. E-mail: gaomy@iccas.ac.cn. F.W.: Mailing address, Medical Isotopes Research Center, Peking University, Xueyuan Road 38, Beijing 100191, China. Fax and tel: 86-10-82801145. E-mail: wangfan@bjum.edu.cn.

† Institute of Chemistry, CAS.

‡ These authors contributed equally to this work.

§ Medical Isotopes Research Center, Peking University.

|| Oncology School of Peking University.

⊥ Cancer Hospital of Chinese Academy of Medical Sciences.

(1) Weissleder, R.; Ntziachristos, V. Shedding light onto live molecular targets. *Nat. Med.* **2003**, *9*, 123–128.

(2) Lee, J. H.; Huh, Y. M.; Jun, Y. W.; Seo, J. W.; Jang, J. T.; Song, H. T.; Kim, S.; Cho, E. J.; Yoon, H. G.; Suh, J. S.; Cheon, J. Artificially engineered magnetic nanoparticles for ultra-sensitive molecular imaging. *Nat. Med.* **2007**, *13*, 95–99.

(3) Weissleder, R.; Pittet, M. J. Imaging in the era of molecular oncology. *Nature* **2008**, *452*, 580–589.

(4) (a) Bruchez, M. J.; Moronne, M.; Gin, P.; Weiss, S.; Alivisatos, A. P. Semiconductor nanocrystals as fluorescent biological labels. *Science* **1998**, *281*, 2013–2016. (b) Chan, W. C.; Nie, S. Quantum dot bioconjugates for ultrasensitive nonisotopic detection. *Science* **1998**, *281*, 2016–2018.

10.1021/mp900143a CCC: $40.75
Published on Web 06/15/2009

enabling the establishment of nanoparticle-based molecular imaging probes for targeting specific disease sites through molecular recognition.

MRI, as a noninvasive tool, has been widely used in the clinic worldwide as it can produce images with extraordinarily high temporal and spatial resolution. It has also been demonstrated that magnetic iron oxide nanoparticles are able to effectively enhance the contrast between normal and pathological tissues. Pioneered by Weissleder, both small particles of iron oxide (SPIO) and ultrasmall particles of iron oxide (USPIO) have received intensive investigations in early tumor *in vivo* detections by either passive or active targeting mode.[2,8−10,16] In the latter mode, various types of targeting molecules are required to conjugate to iron oxide nanoparticles for specifically targeting the receptors expressed on the tumor cell surface. This concept has been proven to be feasible by different groups, consequently raising great research interests of using USPIO-enhanced MRI in early tumor detection *in vivo*.[2,8,9] Yet, the chemical synthesis of biocompatible iron oxide nanoparticles with satisfactory blood circulation time and particle surface functionalizability remain far from optimal. Furthermore, the *in vivo* behaviors of nanoparticles with different surface structures are necessarily subjected to systematic investigations.[17]

In our previous investigations, we have established an innovative synthetic route for achieving water-soluble and biocompatible magnetite nanocrystals via a "one-pot" reaction.[18−20] PEG (poly(ethylene glycol))-coated Fe_3O_4 nanocrystals, as the direct product of the "one-pot" reaction, were demonstrated to be useful in disease detection via either passive mode or active mode.[9,21] Following on from our previous investigations, we have recently been working on the synthesis and *in vivo* applications of a novel type of dual-modality molecular probe designed for tumor detection by both MRI and single-photon emission computed tomography (SPECT). For a molecular imaging tool to be useful, high enough sensitivity, sufficiently high spatial resolution and a high degree of specificity for the target of interest are essentially required. MRI is powerful for its high spatial resolution and tomographic capabilities, but limited by its low signal sensitivities. By contrast, nuclear imaging modalities such as positron emission tomography (PET) and SPECT are characterized by very high sensitivity, up to 10^{-12} mol/L, but with relatively low imaging resolution. Therefore, it is meaningful to design a dual-modality molecular imaging

(5) Gao, X.; Cui, Y.; Levenson, R. M.; Chung, L. W.; Nie, S. *In vivo* cancer targeting and imaging with semiconductor quantum dots. *Nat. Biotechnol.* **2004**, *22*, 969–976.

(6) Wisniewski, T.; Pankiewicz, J.; Scholtzova, H.; Fernando, G.; Chabalgoity, J. A.; Ji, Y.; Wadghiri, Y. Z.; Gan, W. B.; Tang, C. Y.; Turnbull, D. H.; Mathis, C. A.; Kascsak, R.; Klunk, W. E.; Carp, R. I.; Frangione, B.; Sigurdsson, E. M.; Sadowski, M.; Carp, I. Imaging and therapeutic approaches for [beta]-sheet structures in prion and Alzheimer's diseases. *Neurobiol. Aging* **2004**, *25*, S30–S31.

(7) De, V. I.; Lesterhuis, W. J.; Barentsz, J. O.; Verdijk, P.; van, K. J.; Boerman, O. C.; Oyen, W. J.; Bonenkamp, J. J.; Boezeman, J. B.; Adema, G. J.; Bulte, J. W.; Scheenen, T. W.; Punt, C. J.; Heerschap, A.; Figdor, C. G. Magnetic resonance tracking of dendritic cells in melanoma patients for monitoring of cellular therapy. *Nat. Biotechnol.* **2005**, *23*, 1407–1413.

(8) Huh, Y. M.; Jun, Y. W.; Song, H. T.; Kim, S.; Choi, J. S.; Lee, J. H.; Yoon, S.; Kim, K. S.; Shin, J. S.; Suh, J. S.; Cheon, J. *In vivo* magnetic resonance detection of cancer by using multifunctional magnetic nanocrystals. *J. Am. Chem. Soc.* **2005**, *127*, 12387–12391.

(9) Hu, F. Q.; Wei, L.; Zhou, Z.; Ran, Y. L.; Li, Z.; Gao, M. Y. Preparation of Biocompatible Magnetite Nanocrystals for *In Vivo* Magnetic Resonance Detection of Cancer. *Adv. Mater.* **2006**, *18*, 2553–2556.

(10) Sun, C.; Veiseh, O.; Gunn, J.; Fang, C.; Hansen, S.; Lee, D.; Sze, R.; Ellenbogen, R. G.; Olson, J.; Zhang, M. *In vivo* MRI detection of gliomas by chlorotoxin-conjugated superparamagnetic nanoprobes. *Small* **2008**, *4*, 372–379.

(11) Czernin, J.; Phelps, M. E. Positron emission tomography scanning: current and future applications. *Annu. Rev. Med.* **2002**, *53*, 89–112.

(12) (a) Wu, Y.; Zhang, X.; Xiong, Z.; Cheng, Z.; Fisher, D. R.; Liu, S.; Gambhir, S. S.; Chen, X. microPET imaging of glioma integrin {alpha}v{beta}3 expression using ^{64}Cu-labeled tetrameric RGD peptide. *J. Nucl. Med.* **2005**, *46*, 1707–1718. (b) Jia, B.; Shi, J. Y.; Yang, Z.; Xu, B.; Liu, Z. F.; Zhao, H. Y.; Liu, S.; Wang, F. ^{99m}Tc-labeled cyclic RGDfK dimer: Initial evaluation for SPECT imaging of glioma integrin {alpha}v{beta}3 expression. *Bioconjugate Chem.* **2006**, *17*, 1069–1076.

(13) Wang, Y. X.; Hussain, S. M.; Krestin, G. P. Superparamagnetic iron oxide contrast agents: physicochemical characteristics and applications in MR imaging. *Eur. Radiol.* **2001**, *11*, 2319–2331.

(14) (a) Anzai, Y.; Blackwell, K. E.; Hirschowitz, S. L.; Rogers, J. W.; Sato, Y.; Yuh, W. T.; Runge, V. M.; Morris, M. R.; McLachlan, S. J.; Lufkin, R. B. Initial clinical experience with dextran-coated superparamagnetic iron oxide for detection of lymph node metastases in patients with head and neck cancer. *Radiology* **1994**, *192*, 709–715. (b) Ros, P. R.; Freeny, P. C.; Harms, S. E.; Seltzer, S. E.; Davis, P. L.; Chan, T. W.; Stillman, A. E.; Muroff, L. R.; Runge, V. M.; Nissenbaum, M. A.; et al. Hepatic MR imaging with ferumoxides: a multicenter clinical trial of the safety and efficacy in the detection of focal hepatic lesions. *Radiology* **1995**, *196*, 481–488.

(15) Corot, C.; Robert, P.; Idee, J. M.; Port, M. Recent advances in iron oxide nanocrystal technology for medical imaging. *Adv. Drug Delivery Rev.* **2006**, *58*, 1471–1504.

(16) Harisinghani, M. G.; Barentsz, J.; Hahn, P. F.; Deserno, W. M.; Tabatabaei, S.; van, K. C.; de, R. J.; Weissleder, R. Noninvasive detection of clinically occult lymph-node metastases in prostate cancer. *N. Engl. J. Med* **2003**, *348*, 2491–2499.

(17) Qiao, R. R.; Yang, C. H.; Gao, M. Y. Superparamagnetic iron oxide nanoparticles: from preparations to in vivo MRI applications. *J. Mater. Chem.* **2009**, DOI: 10.1039/b902394a.

(18) Li, Z.; Chen, H.; Bao, H. B.; Gao, M. Y. One-pot reaction to synthesize water-soluble magnetite nanocrystals. *Chem. Mater.* **2004**, *16*, 1391–1393.

(19) Hu, F.; Li, Z.; Tu, C.; Gao, M. Y. Preparation of magnetite nanocrystals with surface reactive moieties by one-pot reaction. *J. Colloid Interface Sci.* **2007**, *311*, 469–474.

(20) Li, Z.; Wei, L.; Gao, M. Y.; Lei, H. One-pot reaction to synthesize biocompatible magnetite nanoparticles. *Adv. Mater.* **2005**, *17*, 1001–1005.

(21) Wei, L.; Zhou, G.; Li, Z.; He, L.; Gao, M. Y.; Tan, J.; Lei, H. Detection of toxoplasmic lesions in mouse brain by USPIO-enhanced magnetic resonance imaging. *Magn. Reson. Imaging* **2007**, *25*, 1442–1448.

probe capable of being detected by these complementary imaging techniques for further increasing the diagnostic accuracy.[22,23]

Herein, we report a new dual-modality molecular probe composed of biocompatible Fe_3O_4 nanocrystal, monoclonal antibody and radionuclide. The biocompatible Fe_3O_4 nanocrystals were prepared by modifying our "one-pot" synthetic route established previously.[9,18−20] In similarity, α,ω-dicarboxyl-terminated PEG (HOOC−PEG−COOH) was adopted as the particle surface capping agent for providing the nanocrystal biocompatibility, meanwhile offering free surface carboxylic acid groups for further covalently binding with a targeting molecule,[9,19] i.e., antigastric cancer monoclonal antibody 3H11 (mAb 3H11) in the current investigation. The latter was labeled with radionuclide ^{125}I for SPECT imaging. All the functional components in the dual-modality molecular probe, i.e., Fe_3O_4, PEG, mAb 3H11 and ^{125}I, were chemically bonded together for forming a stable molecular probe. Systematic *in vitro* experiments were carried out for evaluating the biological activity of the antibody in the targeting probe. A series of *in vivo* experiments were performed for detecting xenografted tumors in nude mice by MRI and γ-imaging techniques. The pharmacokinetics of the molecular probe in tumor-bearing nude mice was studied by γ-counter analyses.

Experimental Section

Chemicals. Iron(III) acetylacetonate ($Fe(acac)_3$) was purchased from Aldrich (14024-18-1) and used after 2 times recrystallizations. Analytical grade chemicals such as ethanol, ether, and diphenyl oxide were purchased from Sinopharm Chemical Reagent Beijing, Co., Ltd. Diphenyl oxide was used after further purification by reduced pressure distillation. EDC (1-ethyl-3-(3-dimethylaminopropyl carbodiimide), 39391) and sulfo-NHS (*N*-hydroxysulfosuccinimide sodium salt, 56485) from Fluka and SDS (sodium dodecyl sulfate, L5750) from Sigma were used as received. Iodogen (1,3,4,6-tetrachloro-3α,6α-diphenylglycouril, T0656) was purchased from Sigma-Aldrich and used without further purification. Iodine-125 carrier free radionuclide ($Na^{125}I$ in 0.1 M NaOH) used in this study was purchased from Perkin-Elmer (NEZ033, Perkin-Elmer) at a radioactive concentration of 350 mCi/mL. Antigastric cancer monoclonal antibody 3H11 and human gastric cancer cell line BGC823 were obtained as gifts from the Oncology School of Peking University.[24] Murine immunoglobulin G (mIgG) was purchased from Sigma (I5381). HOOC−PEG−COOH was synthesized according to literature.[20]

Preparation of Biocompatible Fe_3O_4 Nanocrystals. A stock solution of diphenyl oxide (15 mL) containing $Fe(acac)_3$ (0.06 M), HOOC−PEG−COOH (0.12 M, M_n = 2000) and oleylamine (0.24 M) was prepared. After being purged with nitrogen, the reaction mixture was quickly heated up and kept refluxing for 24 h. Then, ether was introduced into the reaction mixture to precipitate the resultant Fe_3O_4 nanocrystals, which were subsequently collected by centrifugation. After that, the precipitate was redissolved in ethanol followed by addition of ether as precipitant. Typically, this purifying procedure was repeated for three cycles. The PEG-coated Fe_3O_4 nanocrystals finally obtained were dissolved in either Milli-Q water or PBS (phosphate buffer saline) for further experiments. The Fe_3O_4 nanocrystals stabilized by HOOC−PEG−COOH have surface carboxylic acid groups available for further covalently conjugating the Fe_3O_4 nanocrystals to molecules bearing amine groups via the EDC/NHS mediated amidation reaction, as demonstrated before.[9,19]

Colloidal Stability of the Biocompatible Fe_3O_4 Nanocrystals. The colloidal stability of the PEG-coated Fe_3O_4 nanocrystals under physiological conditions was studied by the dynamic light scattering (DLS) method. The hydrodynamic sizes of Fe_3O_4 nanocrystals in both physiological saline and fetal bovine serum (FBS, Invitrogen) were monitored and compared with those recorded from Fe_3O_4 nanocrystals prepared in 2-pyrrolidone rather than diphenyl oxide according to a previous report.[9]

Radiolabeling. mAb 3H11 was labeled with ^{125}I using the Iodogen method as previously reported.[25] Briefly, 450 μg of mAb 3H11 (225 μL, 2.0 mg/mL) in phosphate buffer (0.2 M, pH 7.4) and 1.05 mCi of $Na^{125}I$ (3 μL, 350 mCi/mL) were added into a glass vial coated with 20 μg of Iodogen. After 5 min of reaction at room temperature, the resultant 3H11-^{125}I was purified by a PD-10 Sephadex G-25 column (17-0851-01, GE Healthcare) equilibrated with phosphate buffer (0.2 M, pH 7.4) to remove unreacted radioiodide. The radiolabeling yield was 70−85% and radiochemical purity was greater than 98% after purification, resulting in a specific activity of 1.6−2.0 mCi/mg. By a similar recipe, the mIgG-^{125}I was also prepared and purified.

(22) Catana, C.; Wu, Y.; Judenhofer, M. S.; Qi, J.; Pichler, B. J.; Cherry, S. R. Simultaneous acquisition of multislice PET and MR images: initial results with a MR-compatible PET scanner. *J. Nucl. Med.* **2006**, *47*, 1968–1976.

(23) DeNardo, S. J.; DeNardo, G. L.; Natarajan, A.; Miers, L. A.; Foreman, A. R.; Gruettner, C.; Adamson, G. N.; Ivkov, R. Thermal dosimetry predictive of efficacy of ^{111}In-ChL6 nanoparticle AMF-induced thermoablative therapy for human breast cancer in mice. *J. Nucl. Med.* **2007**, *48*, 437–444.

(24) (a) Guo, J.; Jin, G.; Meng, L.; Ma, H.; Nie, D.; Wu, J.; Yuan, L.; Shou, C. Subcellullar localization of tumor-associated antigen 3H11Ag. *Biochem. Biophys. Res. Commun.* **2004**, *324*, 922–930. (b) Chen, D.; Shou, C. Molecular cloning of a tumor-associated antigen recognized by monoclonal antibody 3H11. *Biochem. Biophys. Res. Commun.* **2001**, *280*, 99–103.

(25) Salacinski, P. R.; McLean, C.; Sykes, J. E.; Clement-Jones, V. V.; Lowry, P. J. Iodination of proteins, glycoproteins, and peptides using a solid-phase oxidizing agent, 1,3,4,6-tetrachloro-3 alpha,6 alpha-diphenyl glycoluril (Iodogen). *Anal. Biochem.* **1981**, *117*, 136–146.

Fe_3O_4−3H11 Conjugates. The conjugation reaction between Fe_3O_4 nanocrystals and mAb 3H11 was performed at 4 °C. Typically, EDC (2.50 μmol) and sulfo-NHS (6.25 μmol) were dissolved in 830 μL of 0.01 M PBS buffer solution containing 2.63 mg of Fe_3O_4 nanocrystals. After approximately 15 min, 380 μL of 0.01 M PBS buffer solution containing 1.27 mg of mAb 3H11 was introduced. Typically, the reaction lasted for 10 h. The conjugate of Fe_3O_4−mIgG was prepared in a similar way and used as a control throughout the following *in vitro* and *in vivo* experiments. By replacing mAb 3H11 with 3H11-^{125}I or replacing mIgG with mIgG-^{125}I, the Fe_3O_4−3H11-^{125}I and Fe_3O_4−mIgG-^{125}I probes were prepared, respectively.

Cell Culture and Animal Models. BGC823 Cells were grown in RPMI-1640 medium supplemented with 10% (v/v) FBS at 37 °C in an atmosphere containing 5% CO_2. The BGC823 tumor model was generated by subcutaneous injection of ~5 × 10^6 cells into proximal thigh and right upper flank regions of female BALB/c nude mice (4−5 weeks old). The mice were used for *in vivo* studies when the tumor volume reached about 200−300 mm^3 (~10 days after inoculation). All the animal experiments were performed according to a protocol approved by the Peking University Institutional Animal Care and Use Committee.

Competitive Binding Assay. BGC823 cells were seeded in the wells of 24-well plates (1 × 10^5 cells/well) and incubated overnight at 37 °C to allow a firm adherence. After being rinsed twice with PBS buffer, the cells were incubated with 3H11-^{125}I (0.15 μCi) at 4 °C for 2 h in the presence of either Fe_3O_4−3H11 or mAb 3H11 with an increasing concentration (0−1000 nM) in binding buffer (0.01 M PBS, pH 7.4, 1% bovine serum albumin). The total incubation volume was adjusted to 200 μL. After that, the cells were rinsed three times with cold PBS buffer and then lysed with 2 M NaOH at room temperature. The cell-associated radioactivity was determined using a γ-counter (Wallac 1470-002, Perkin-Elmer). The half maximal inhibitory concentrations (IC_{50}) of mAb 3H11 and Fe_3O_4−3H11 to BGC823 cells against 3H11-^{125}I were determined by fitting the data with nonlinear regression using GraphPad Prism (version 4.0, GraphPad Software, Inc.). All experiments were repeated twice with triplicate samples.

Binding Specificity. The BGC823 cells were harvested, rinsed three times with PBS, and resuspended in the binding buffer. Then, the cells were divided into three groups (1 × 10^7 cells per group). In the first group, the cells were incubated with Fe_3O_4−3H11-^{125}I probe (0.02 μCi), while the cells in the second group were incubated with Fe_3O_4−3H11-^{125}I probe (0.02 μCi) in the presence of excessive mAb 3H11 (1000 folds of the probe), and the tumor cells in the last group were incubated with equivalent amount of Fe_3O_4−mIgG-^{125}I (0.02 μCi) in the absence of pure mAb 3H11. The total incubation volume was 1 mL. After being gently rotated overnight at 4 °C, the cells were washed and the cell-associated radioactivity was determined by γ-counter. Experiments were performed with triplicate samples per group.

***In Vitro* MRI.** For the *in vitro* MRI experiments, 6 × 10^7 BGC823 cells were trypsinized with 0.25% of trypsin solution for 3 min at 37 °C, and washed twice with PBS, then resuspended in binding buffer (2 × 10^6 cells/mL). Afterward they were incubated in triplicate with Fe_3O_4−3H11-^{125}I, Fe_3O_4−mIgG-^{125}I, or Fe_3O_4 (80 μg of Fe_3O_4/group) overnight at 4 °C, respectively. After being thoroughly washed with cold PBS buffer, the cells were lysed by 300 μL of 10% SDS. MRI measurements were carried out on a 3 T clinical MRI instrument (GE signa 3.0T HD, Milwaukee, WI). The parameters were set as follows: field of view (FOV) = 10 × 10 cm^2; matrix size = 192 × 192; slice thickness = 1 mm; echo time (TE) = 25, 50, 109 ms; repetition time (TR) = 2100 ms; number of excitations (NEX) = 8.

***In Vivo* MRI.** Nude mice bearing BGC823 tumor xenografts implanted at their proximal thigh and right upper flank regions were anesthetized and then injected via tail vein with Fe_3O_4−3H11-^{125}I or Fe_3O_4−mIgG-^{125}I [(16.8 mg of Fe)/(kg of body weight), n = 3/group]. At 10 min, 2 h, 4 h, 8 h, 12 h, 16 h, 24 h, 48 and 72 h postinjection, the mice were subjected to the *in vivo* MR imaging. For image acquisition, a 1 in. animal quadrature coil, developed by MR Modality of GE HealthCare, China, was used. The detailed imaging parameters were set as follows: FOV = 8 × 8 cm^2; matrix size = 160 × 128; slice thickness = 1 mm; TE = 120 ms; TR = 2500 ms; and NEX = 4.

γ-Imaging. γ-Imaging studies were performed as previously reported.[12b] Briefly, the nude mice bearing BGC823 tumor xenografts were anesthetized and then injected via tail vein with either Fe_3O_4−3H11-^{125}I or Fe_3O_4−mIgG-^{125}I [10 mCi/(kg of body weight), corresponding to injection dose of (16.8 mg of Fe)/(kg of body weight); n = 3/group]. The mice were imaged by using a two-head γ-camera (SIEMENS, E. CAM) equipped with a low energy high resolution (LEHR) parallel hole collimator. At 10 min, 4 h, 14 h, 24 h, 48 h, 72 and 96 h postinjection, planar images were acquired and stored digitally in a 128 × 128 matrix. The acquisition count limits were set at 100 k. For each image, regions of interest (ROI) were drawn over the tumors as well as the whole body of each mouse. The radio counts were obtained by summing up the counts from all pixels within ROI. For more quantitative analysis, 1% of injected dose of Fe_3O_4−3H11-^{125}I was used as an internal reference and imaged simultaneously at each image acquisition time point.

Biodistribution. For the biodistribution study, animals were anesthetized by intraperitoneal injection of sodium pentobarbital at a dose of 45.0 mg/kg. Then, the Fe_3O_4−3H11-^{125}I or 3H11-^{125}I (10 μCi per mouse) was intravenously injected into BGC823 tumor-bearing mice. Animals were sacrificed at 10 min, 14 h, 24 h, 48 and 72 h postinjection, respectively (n = 4/group). Tumor tissues and other organs of interest (such as blood, heart, liver, spleen, kidney, and stomach) were harvested and measured for radioactivity in a γ-counter. The organ uptake was calculated and expressed in percentage injected dose per organ (% ID/organ).

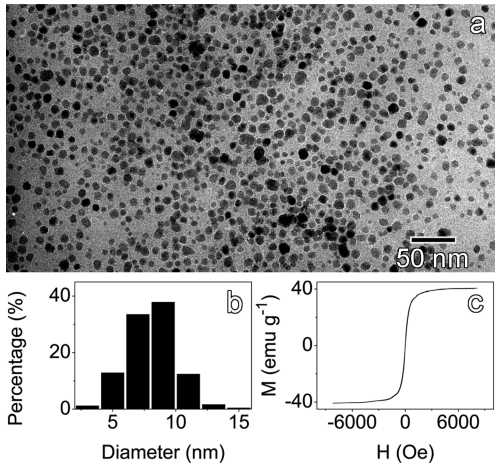

Figure 1. (a) TEM image, (b) histogram, and (c) room-temperature magnetization curve of the as-prepared PEG-coated Fe_3O_4 nanocrystals.

Results and discussion

In our previous investigations, we have demonstrated that biocompatible Fe_3O_4 nanocrystals can be prepared via the pyrolysis of $Fe(acac)_3$ in 2-pyrrolidone in the presence of various types of carboxyl-terminated PEG.[9,20] In those preparations, 2-pyrrolidone not only offers a high enough reaction temperature for pyrolyzing $Fe(acac)_3$ but also serves as a coordinating solvent.[18,19] Nevertheless, due to the small molecular size it does not offer strong enough hindrance effect to the resultant nanocrystals dispersed in solution.[17] Therefore, to further enhance the colloidal stability of the resultant nanocrystals in physiological saline and serum, the synthetic approach was modified in the current investigation by replacing the strong polar solvent 2-pyrrolidone with nonpolar diphenyl oxide. In addition, oleylamine was also used to costabilize the resultant nanocrystals together with α,ω-dicarboxyl-terminated PEG ($M_n = 2000$). More details on the chemical synthesis of these new types of particles will be published elsewhere.

The resultant PEG-coated Fe_3O_4 nanocrystals were characterized by transmission electron microscopy (TEM) and electron diffraction (data not shown). A representative TEM image given in Figure 1a shows the general morphology of the resultant nanocrystals. Their size distribution is depicted by the histogram shown in Figure 1b. The number-average particle size was determined to be of 8.1 nm by measuring more than 300 particles. Electron diffraction experiments suggested that the particles shown in Figure 1a are magnetite nanocrystals. The room-temperature magnetization curve shown in Figure 1c further demonstrates that the PEG-coated Fe_3O_4 nanocrystals are superparamagnetic with a saturation magnetization of 40.4 emu/g, corresponding to 55.8 emu/(mass of Fe).

Satisfying colloidal stability of the Fe_3O_4 nanoparticles is greatly important with respect to *in vivo* applications of Fe_3O_4 nanoparticles as MRI contrast agents. Poor colloidal stability will surely lead to short blood half-time, which is therefore not suitable for constructing molecular probes.[17] In the worst

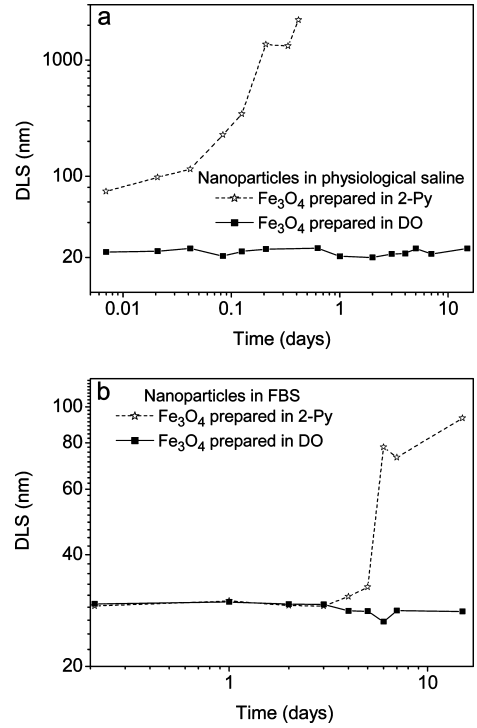

Figure 2. Temporal evolutions of the hydrodynamic sizes of the PEG-coated Fe_3O_4 nanocrystals synthesized in 2-pyrrolidone (2-Py) and diphenyl oxide (DO), respectively.

case, the agglomeration of colloidal particles in blood can also cause vascular embolism as colloidal particles tend to aggregate in salt environment. To show the enhanced colloidal stability of the Fe_3O_4 nanoparticle sample presented in Figure 1, another PEG-coated Fe_3O_4 nanoparticle with comparable size was prepared in 2-pyrrolidone instead of diphenyl oxide according to one of our previous publications.[9] The colloidal stability of these two nanocrystal samples in physiological saline (0.9% NaCl) and fetal bovine serum (FBS) was investigated by the DLS method. The temporal evolutions of the hydrodynamic size of these two samples are shown in Figure 2. In physiological saline, the Fe_3O_4 nanocrystals prepared in 2-pyrrolidone quickly flocculate with hydrodynamic size increasing to >300 nm within two hours, and obvious precipitation was practically observed in several hours. In contrast, the Fe_3O_4 nanocrystals prepared in diphenyl oxide presented an excellent stability with the hydrodynamic size being nearly unchanged for more than 2 weeks. In FBS, the nanoparticles prepared in 2-pyrrolidone present an increased stability but start to flocculate after 4 days, while the nanoparticles shown in Figure 1 keep stable for more than 2 weeks. All these observations strongly demonstrate that current synthetic protocol offers biocompatible Fe_3O_4 nanoparticles with greatly improved colloidal stability both in physiological saline and in FBS.

The Fe_3O_4 nanoparticle-based dual-modality molecular probe was prepared by two different routes. In the first route, mAb 3H11 was first conjugated to Fe_3O_4 nanocrystal through α,ω-dicarboxyl-terminated PEG chemically bonded on the particle surface,[19,20] then labeled with ^{125}I by the Iodogen

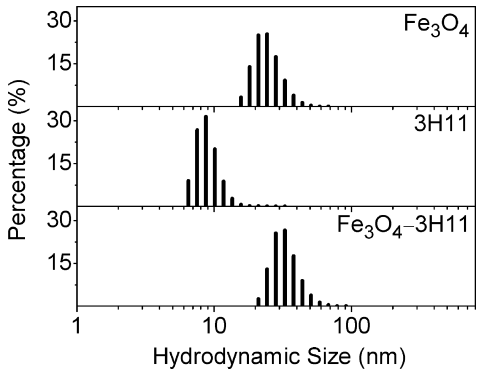

Figure 3. Size distribution profiles of (a) PEG-coated Fe_3O_4 nanocystals, (b) mAb 3H11, and (c) Fe_3O_4−3H11 conjugate determined by dynamic light scattering.

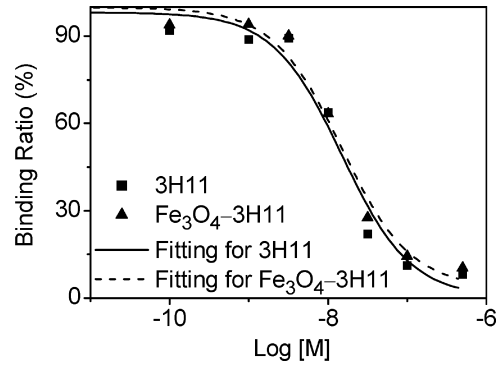

Figure 4. Experimental results accompanied by a theoretical fitting for competitive binding assays.

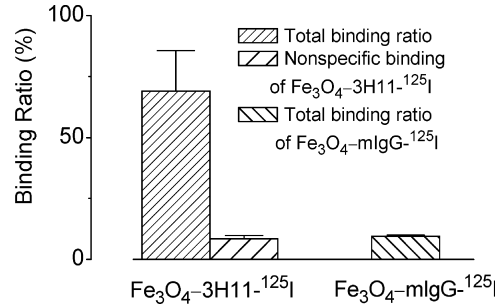

Figure 5. Specific binding of Fe_3O_4−3H11-^{125}I (left) and Fe_3O_4−mIgG-^{125}I (right) to BGC823 cells, respectively. The nonspecific binding for Fe_3O_4−3H11-^{125}I (left-middle) was obtained by competitive binding assay carried out in the presence of excess mAb 3H11.

method. In the second route, mAb 3H11 was first labeled with ^{125}I, then conjugated to the PEG-coated Fe_3O_4 nanocrystals as mentioned in the Experimental Section. In practice, both of these two synthetic routes had nearly the same effectiveness except that, by the first synthetic route, a purification process prior to radiolabeling was required to remove impurities, introduced by the conjugation reaction mediated by EDC and sulfo-NHS, which interfered with the following radiolabeling reaction. Therefore, the latter synthetic route was adopted for preparing Fe_3O_4−3H11-^{125}I and Fe_3O_4−mIgG-^{125}I probes.

The coupling reaction between mAb 3H11 and the PEG-coated Fe_3O_4 nanocrystal was first investigated by dynamic light scattering method. The results shown in Figure 3 reveal that the initial hydrodynamic size of Fe_3O_4 and mAb 3H11 is 24.9 and 9.0 nm, respectively. In contrast, the hydrodynamic size of the resultant conjugate increases to 33.5 nm. Furthermore, the size distribution profile of the conjugates remains nearly unchanged in comparison with those for Fe_3O_4 and mAb 3H11. The reasonable variation in the hydrodynamic size of Fe_3O_4 particles before and after the coupling reaction strongly suggests that mAb 3H11 is effectively coupled to the PEG-coated Fe_3O_4 nanoparticles via the EDC/sulfo-NHS-mediated amidation reaction. Most importantly, there is only one peak present in the size distribution profile of the Fe_3O_4−3H11 conjugate, implying that no coagulation occurred during the conjugation reaction taking place in 0.01 M PBS.

The conjugate was further analyzed by the electrophoresis method.[9] As shown in the Supporting Information, the Fe_3O_4−3H11 conjugate presents different electrophoretic behavior in comparison with mAb 3H11, which further supports that mAb 3H11 has been effectively coupled to the PEG-coated Fe_3O_4 nanocrystals through the conjugation reaction.[9,19]

Maximally maintaining the bioactivity of mAb 3H11 in the Fe_3O_4−3H11 conjugate is one of the most essential issues for the following experiments. Therefore, the bioactivity of mAb 3H11 in the Fe_3O_4−3H11 conjugate was quantitatively evaluated through competitive binding assays as described in the Experimental Section. Detailed results are shown in Figure 4. The theoretical fitting results reveal that the IC_{50} (50% inhibitory concentration) value for the Fe_3O_4−3H11 is 14.9 nmol/L, quite close to 14.8 nmol/L for mAb 3H11, suggesting that the biological activity of mAb 3H11 is well preserved after the conjugation reaction.

The binding specificity of Fe_3O_4−3H11-^{125}I was evaluated by comparing with Fe_3O_4−mIgG-^{125}I which was supposed to have no binding specificity to BGC823 cells. In detail, two equal amounts of BGC823 cells were incubated respectively with Fe_3O_4−3H11-^{125}I and Fe_3O_4−mIgG-^{125}I with the same radioactive counts. After the cells were thoroughly washed with cold PBS buffer, the cell-associated radioactivity was measured. The radioactivity of cells treated with Fe_3O_4−3H11-^{125}I was determined to be 69.0 ± 16.3% of initial radioactivity. In contrast, the radioactivity remaining was only 9.5 ± 0.4% with respect to the negative control, Fe_3O_4−mIgG-^{125}I, as shown in Figure 5. This huge difference strongly suggests that the Fe_3O_4−3H11-^{125}I probe possesses a high binding specificity. Further competitive binding experiment reveals that the binding radioactivity in the former system dropped to 8.5 ± 1.3% in the presence of excess mAb 3H11, quite close to the nonspecific binding radioactivity for Fe_3O_4−mIgG-^{125}I. Supposing that 69.0 ± 16.3% of the initial radioactivity corresponds to the saturated surface binding situation with respect to Fe_3O_4−3H11-^{125}I, the inherent nonspecific binding ratio of the nanoprobes composed of Fe_3O_4 and mIgG should be below 15% derived from the nonspecific binding results for Fe_3O_4−mIgG-^{125}I.

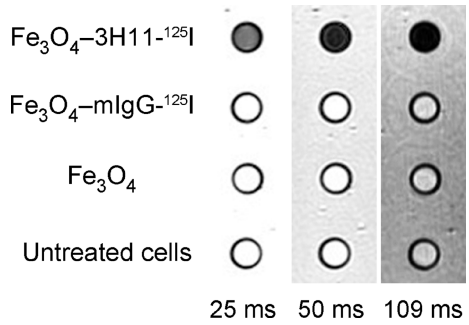

Figure 6. T2-weighted MR images of lysed BGC823 cells treated with Fe_3O_4−3H11-^{125}I, Fe_3O_4−mIgG-^{125}I, and Fe_3O_4, respectively; the sample on the bottom is the untreated cell sample for comparison.

The above-mentioned results allowed further *in vitro* MRI experiments to assess the targeting ability of the dual-modality molecular probe to human gastric cancer cell line (BGC823). For comparison, Fe_3O_4−mIgG-^{125}I was used as a negative control. Four equal portions of a BGC823 cell solution were prepared, and three of them were used to incubate with Fe_3O_4−3H11-^{125}I, Fe_3O_4−mIgG-^{125}I, and the PEG-coated Fe_3O_4 nanocrystals, respectively. The fourth cell sample was also subjected to the same incubation conditions simply for comparison. After being thoroughly washed with cold PBS buffer to remove unbound Fe_3O_4 particles, the cell samples were lysed and subjected to MRI experiments. Figure 6 presents spin−spin relaxation time (T2)-weighted MR images of these four samples acquired by different echo time. It is quite evident that only the cell sample treated with Fe_3O_4−3H11-^{125}I presents a strongly enhanced MRI signal, suggesting that the Fe_3O_4−3H11-^{125}I probe can specifically target BGC823 cells. From the signal intensity measured at different echo times, the longitudinal relaxivity was calculated to be 14.62 s^{-1}.

On the basis of the aforementioned systematic characterizations as well as successful *in vitro* experiments, Fe_3O_4−3H11-^{125}I was used in the following experiments for *in vivo* detecting tumors in BALB/c nude mice bearing BGC823 human gastric cancer xenografts implanted at their proximal thigh and right upper flank regions. Fe_3O_4−mIgG-^{125}I served as a negative control. T2-weighted MR images acquired before and at different time points after injection of Fe_3O_4−3H11-^{125}I or Fe_3O_4−mIgG-^{125}I are shown in Figure 7a. More quantitative results on the temporal variations of T2 values are given in Figure 7b. In general, the T2 value of tumor starts to decrease 4 h after the injection of Fe_3O_4−3H11-^{125}I, reaching a minimum at 24 h by a decrease of ∼30%, and then increases. However, the hypointensive T2 signal remains throughout the whole inspected time window. With respect to the control experiment, a decreased T2 value of the tumor also appears but with a much lower T2 decrease (<10%), which is probably caused by the nonspecific binding of Fe_3O_4−mIgG-^{125}I to tumor cells as demonstrated by *in vitro* experiments. However, the T2 value of the tumor completely recovers 60 h after the administration of Fe_3O_4−mIgG-^{125}I. The significant difference between T2 enhancing effects caused by Fe_3O_4−3H11-^{125}I and Fe_3O_4−mIgG-^{125}I, respectively, clearly demonstrates that the dual-modality molecular probe possesses specific targeting ability to tumor via the interaction between the targeting molecule and the receptor expressed on tumor cells. Even though Fe_3O_4−mIgG-^{125}I also gives rise to a weaker hypointensive T2 signal, which is a subject of our ongoing study, the latter part of the time window for T2 signal enhanced by Fe_3O_4−3H11-^{125}I remains available for unambiguously identifying tumor. In comparison with our previous investigations,[9] the general variation of T2 value presents a rather similar behavior during the first 24 h postinjection. But the maximal variation of T2 value in the current case reaches ∼30%, much higher than that (∼10%) observed in our previous investigations.[9] This improved MR enhancing effect is undoubtedly attributed to the new synthetic route which produces nanoparticles with much improved biocompatibility. For example, by doping iron oxide particles with different types of transition metals such as Mn^{2+}, Fe^{2+}, Co^{2+}, and Ni^{2+}, Suh and Cheon have invented a series of "magnetism-engineered" iron oxide (MEIO) particles. Among them, $MnFe_2O_4$ particles present the highest magnetic susceptibility. Nevertheless, the R2 (relativity value being equal to 1/T2) enhancement factor based on $MnFe_2O_4$ particles is only 31% in *in vivo* tumor detection.[2] By converting the maximum T2 enhancement factor of the current dual-modality probe to R2 enhancement factor, ΔR2 reaches ∼42%. Most importantly, the hypointensive T2 signal observed in the current investigation keeps increasing until 24 h postinjection, suggesting that the PEG-coated Fe_3O_4 nanocrystals prepared by the current synthetic route possess greatly improved circulating behavior in blood.

Since nuclear imaging techniques including PET and SPECT offer much higher sensitivity than MRI, therefore, it is practically meaningful to develop nuclear-MR dual-modality molecular imaging probes for more unambiguously detecting early stage tumors as well as other types of diseases. We chose ^{125}I as radionuclide in the current investigations due to the following reasons: (1) ^{125}I can be used for SPECT imaging for animal experiments; (2) it also offers a sensitive approach for tracing the *in vivo* behaviors of the nanocrystals with different size and surface structure, which will provide important feedback for optimizing the nanoparticle-based imaging probes; (3) it is relatively safer to handle; (4) the established synthetic protocol can easily be extended to other iodine isotopes, such as ^{123}I, ^{124}I, and ^{131}I, which are useful not only for SPECT and PET imaging but also for radiotherapy. With respect to the current investigations, to crosscheck the *in vivo* tumor imaging results based on MRI experiments, another group of tumor-bearing nude mice was chosen for γ-imaging upon injections of Fe_3O_4−3H11-^{125}I with Fe_3O_4−mIgG-^{125}I being used as control. Representative images acquired at 10 min, 14 h, 24 h, 48 h, and 72 h postinjection were selected and are shown in Figure 7c. 1% of the injected dose of Fe_3O_4−3H11-^{125}I was placed in the top middle of each image as a reference for analyzing the imaging results. Quantitative data extracted

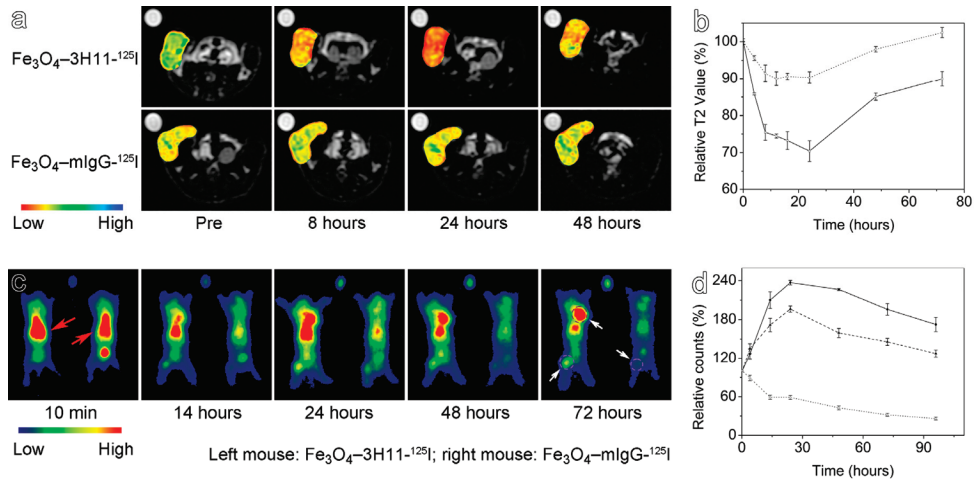

Figure 7. (a) T2-weighted MR images of tumor-bearing nude mice acquired before and at different time points after intravenous injections of Fe_3O_4−3H11-^{125}I and Fe_3O_4−mIgG-^{125}I, respectively. (b) Variations of T2 values of tumors after the injections of Fe_3O_4−3H11-^{125}I (solid line) and Fe_3O_4−mIgG-^{125}I (dotted line), respectively. (c) γ-Images of tumor-bearing nude mice captured at different times postinjection. (d) The normalized γ-counts extracted after injection of Fe_3O_4−3H11-^{125}I from the whole body (dotted line), the tumor at upper flank region (solid line), and the tumor at proximal thigh region (dashed line) of the mouse at the left-hand side in each image, by using 1% injection dose (top middle) as internal reference. Both MR and γ-images are color-coded for better showing the tumors.

from the images are shown in Figure 7d. It is quite obvious that the dual-modality molecular probe can effectively target the tumors implanted at both proximal thigh and right upper flank regions. The γ-signals of tumors in the experimental group are much more intensive than that in the control group. Moreover, the general targeting behavior of Fe_3O_4−3H11-^{125}I is well in consistence with that obtained by MRI.

Apart from providing the signal from tumor sites, the γ-imaging experiments also offer the possibility to monitor the biodistribution and *in vivo* characteristics of the nanoprobes, which is difficult to achieve solely by MRI. The results shown in Figure 7c as well as more parallel control studies not shown here reveal that the Fe_3O_4-based probes are quickly distributed in liver within the first 10 min after injection. Then, the nanoparticle probes start to be washed out of liver and give rise to detectable accumulation at tumor sites approximately 14 h postinjection. Eventually, the molecular probe distributed more in tumor than in liver. As liver is a blood-rich organ, the initial quick distribution in liver suggests that there are almost no nanoparticle probes stacked in the bloodstream due to the possible coagulation caused by their interactions with serum proteins and blood cells. The following decay of the liver signal together with the signal increase in tumors implies that the current Fe_3O_4 nanocrystal possesses excellent stealth nature, which is essential for *in vivo* molecular imaging upon the use of nanoparticle-based molecular probes. It is also worthy of mentioning that the whole body γ-counts decrease against time, suggesting that at least ^{125}I is being eliminated against time. It is interesting to ask how these nanoprobes are metabolized. Note that in the γ-images shown in Figure 7 as well as those not being presented, the bladder starts to show γ-signal shortly after the injection of the probes. Therefore, the urine was collected after the injection of the probes and then subjected to TEM measurements. It was confirmed that Fe_3O_4 nanoparticles were present in urine.

To provide more accurate biodistribution information on the Fe_3O_4−3H11-^{125}I probe, tumor tissues and other organs of interest, including blood, heart, liver, spleen, kidney, and stomach, were harvested from BGC823 tumor-bearing mice at different time points postinjection, and then the radioactivity of the tumor tissues as well as the aforementioned organs was determined by γ-counter. The results shown in Figure 8a demonstrate that the Fe_3O_4−3H11-^{125}I probe is heavily distributed in liver within 10 min (by 38.4 ± 3.6%) apart from being in blood (by 51.2 ± 6.8%). From then on, the liver uptake of the probe keeps decreasing within the inspected time window. Meanwhile, the tumor uptake of the probe quickly increases within 24 h postinjection to 4.1 ± 0.6% and reaches a maximum of 4.7 ± 0.7% at 48 h postinjection. Eventually, the molecular probe is distributed more in tumor than in liver. For comparison, the biodistribution behavior of 3H11-^{125}I was also investigated. The results shown in Figure 8b suggest that the general behavior of the Fe_3O_4−3H11-^{125}I probe follows that of 3H11-^{125}I except that the former one presents slightly heavier distribution in liver, which is probably caused by the bigger size of the Fe_3O_4−3H11-^{125}I probe. It is worthy of mentioning that there is a huge percentage of the molecular probe remaining in blood at the third day postinjection, suggesting that the current dual-modality molecular probe possesses excellent circulating behavior in blood.

The results shown in Figure 8 strongly support the general pharmacokinetics behavior of the Fe_3O_4−3H11-^{125}I probe extracted from both MRI (Figure 7b) and γ-imaging measurements (Figure 7d). The only discrepancy is that the results shown in Figure 8 suggest that the tumor uptake of the dual-modality molecular probe reaches its maximum at

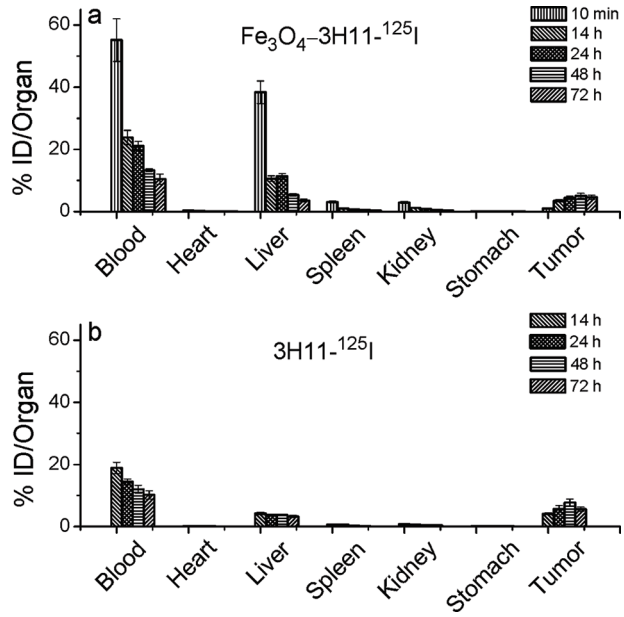

Figure 8. Organ uptake (% ID/organ) of (a) Fe_3O_4−3H11-^{125}I at 10 min, 14 h, 24 h, 48 and 72 h, and (b) 3H11-^{125}I at 14 h, 24 h, 48 h, and 72 h in nude mice ($n = 4$) bearing the BGC823 tumor xenografts.

48 h postinjection, while the biodistribution extracted from γ-imaging results suggests that 24 h is the time for the maximal uptake of the molecular probe by tumors. This discrepancy can partly be attributed to the fact that to extract the biodistribution information of the molecular probe based on the γ-imaging results, as described herein, is only a semiquantitative approach. Moreover, one should notice that the pharmacokinetic curves obtained by both methods are characterized by relatively flat peaks. With respect to the MRI experiments, the reasons for the T2 value to reach its minimum at 24 h postinjection rather than 48 h are rather complicated as the MRI signal is an integrative function of the particle concentration, aggregation degree, and the following degradation of the Fe_3O_4−3H11-^{125}I probe within tumor tissues.

In summary, we have successfully developed a novel type of dual-modality molecular probe for *in vivo* detection of tumor by both MRI and SPECT. In this molecular probe, all components, Fe_3O_4 nanocrystal, PEG, mAb 3H11, and ^{125}I, are chemically bonded together. Benefiting from the PEG-coated Fe_3O_4 nanoparticles prepared via a modified "one-pot" synthetic route based on our previous investigations, the dual-modality molecular probe presents a strongly enhanced MR contrast effect in comparison with previous literature results. Moreover, the sensitive γ-imaging results based on the covalently attached ^{125}I not only support the MR imaging results but also provide additional information on biodistribution of the dual-modality probe, therefore offering a sensitive approach for evaluating the *in vivo* behaviors of nanoparticle-based molecular probes. It is also worthy of mentioning that the current MR and γ-imaging results are obtained with the aid of clinic imaging facilities, which would be helpful for pushing the nanoparticle-based molecular probes to clinical applications even though the imaging quality is sacrificed in comparison with those acquired by 4.7 or 9.4 T animal MRI instruments. Most importantly, the current synthetic protocol can easily be extended to PET-MR imaging agent, even imaging-therapy combined nanomedicine by using different radioisotopes of iodine.

Acknowledgment. The current investigations are jointly supported by NSFC projects (20773140, 20640430564, 20820102035, 30870728) and an 863 project (2007AA02Z467). The authors are grateful to the MR Modality of GE HealthCare, China, for their great help in establishing a one-inch quadrature coil for animal MRI experiments. The help from Ms. Huiyun Zhao and Mr. Cunjing Jin with respect to animal experiments is also appreciated. The authors thank Dr. Dayang Wang from MPIKG for stimulating discussions.

Supporting Information Available: Electrophoresis experimental results. This material is available free of charge via the Internet at http://pubs.acs.org.

MP900143A